Polymorphs of Ln_2MoO_6: A Neutron Diffraction Investigation of the Crystal Structures of La_2MoO_6 and Tb_2MoO_6

J. S. Xue, Mark R. Antonio, and L. Soderholm*

Chemistry Division, Argonne National Laboratory, Argonne, Illinois 60439-4831

Received August 15, 1994. Revised Manuscript Received October 26, 1994[⊗]

The structures exhibited by the compounds Ln_2MoO_6 (Ln = La–Tb) are found to be influenced by synthetic conditions. Crystal structures of two of the three observed polymorphs (γ and α; Ln = La and Tb) have been refined from time-of-flight powder-neutron-diffraction data. The diffraction data obtained from La_2MoO_6 are inconsistent with the previously reported space group $I\bar{4}2m$ but refine well in $I4_1/acd$ (No. 142). There is no direct evidence in the data to support previous indications that the cell is acentric. The set of $(21l)$ reflections are considerably broadened, and this has been characterized using a stacking fault model with a boundary dimension of every 2.5 unit cells perpendicular to the c axis. Implications of these results are discussed in terms of physical properties, structural relationships, and polymorphic phase transitions within the Ln_2MoO_6 series.

Introduction

Ln_2MoO_6 (Ln = lanthanides and Y) compounds are of interest because of their potential applications in catalysis. They have been reported to crystallize in three polymorphs with monoclinic (α), cubic (β), or tetragonal (γ) symmetries, depending on the size of Ln and the synthetic conditions.[1] The large (or light) lanthanides usually crystallize in structures with cubic (β) or tetragonal (γ) symmetries, whereas most of the small or heavy lanthanides (Sm–Lu) form with a monoclinic (or α) phase under normal synthetic conditions. The monoclinic phase is closely related to the scheelite-type compound Bi_2MoO_6, an extensively used catalytic component for selective olefin oxidation.[2]

The crystal structure of La_2MoO_6 was first reported[3] as tetragonal (γ) with a = 4.089 Å, c = 15.99 Å and assigned the acentric space group $I\bar{4}2m$ (No. 121). However, there are additional weak peaks in the X-ray diffraction pattern of powdered La_2MoO_6 single crystals[4,5] that cannot be indexed using the unit cell reported in ref 3. Efremov et al.[5] reinvestigated the La_2MoO_6 structure by single-crystal X-ray diffraction and reported a different cell for the γ phase, based on a cell $\sqrt{2}$ times the originally assigned, $I\bar{4}2m$ a axis and a doubling of the c axis to result in an a axis equal to 5.798 Å and a c axis of 32.036 Å. They reported that the simplest model to fit their data had symmetry consistent with the centric space group $I4_1/acd$ (No. 142). However, the independent report[6] of a weak piezoelectric effect lead Efremov et al. to refine the data in the acentric subgroup $I\bar{4}c2$ (No. 120). Overall, the refinement in the acentric space group did not appreciably improve the fit.

The crystal structure of the monoclinic α phase was first determined for the tungstate compounds Ln_2WO_6 (Ln = Nd or Gd).[7,8] The α polymorph of Ln_2MoO_6, as typified by the Sm and Gd analogues, has been reported in two different settings of space group No. 15: $I2/c$ and $C2/c$.[1,7] These two settings lead to slightly different a-axis lengths and β angles. The structural relationship between the α phase and the monoclinic scheelite structure is simply $a \approx 3a_s \approx 15.9$ Å, $b \approx c_s \approx 11.4$ Å, $c \approx b_s \approx 5.5$ Å, $\beta \approx \beta_s \approx 91°$. The crystal structure of Tb_2MoO_6 has thus far been assumed to be isostructural with the Sm and Gd molybdates.

The structure of the β phase is realized in Ce_2MoO_6. The details of this structure remain unknown although "fluorite-like" or "cubic" is used extensively in the literature to describe the structure.[9,10] Whereas the major peaks in an X-ray powder pattern can be indexed on a simple fluorite cell (5.5544 Å, $Fm3m$),[11] there is evidence of weak additional reflections. Neutron diffraction data, taken on the same sample, reveal these additional reflections much more clearly.[12] In addition, X-ray absorption fine structure (XAFS) results[13] demonstrate that cerium and molybdenum ions do not disorder, as required in the simple fluorite structure, but instead occupy distinct crystallographic sites.[13,14]

[⊗] Abstract published in *Advance ACS Abstracts,* January 15, 1995.

(1) Klevtsov, P. V.; Kharchenko, L. Y.; Klevtsova, R. F. *Sov. Phys. Crystallogr.* **1975**, *20*, 349.
(2) Buttrey, D. J.; Vogt, T.; Wildgruber, U.; Robinson, W. R. *J. Solid State Chem.* **1994**, *111*, 118.
(3) Sillen, L. G.; Lundborg, K. *Z. Anorg. Chem.* **1943**, *252*, 2.
(4) Brixner, L. H.; Sleight, A. W.; Licis, M. S. *J. Solid State Chem.* **1972**, *5*, 186.
(5) Efremov, V. A.; Tyulin, A. V.; Trunov, V. K. *Sov. J. Coord. Chem.*, **1987**, *13*, 721.
(6) Morozov, N. N.; Muravev, E. N.; Gokhman, L. Z.; Lysanova, G. V.; Ivanova, M. M.; Reznik, E. M.; Spiridonov, E. G.; Karpushkina, G. I. *Izv. Akad. Nauk SSSR, Neorg. Mater.* **1975**, *11*, 2000.
(7) Tyulin, A. V.; Efremov, V. A. *Sov. Phys. Crystallogr.* **1987**, *32*, 215.
(8) Polyanskaya, T. M.; Borisov, S. V.; Belov, N. V. *Sov. Phys. Crystallogr.* **1971**, *15*, 636.
(9) Brixner, L. H. *Rev. Chim. Mineral.* **1973**, *10*, 47.
(10) Manthiram, A.; Gopalakrishnan, J. *J. Less-Common Met.* **1984**, *99*, 107.
(11) Xue, J. S., 1993, unpublished.
(12) Soderholm, L.; Beno, M. A.; Eastman, J.; Antonio, M. R.; Xue, J. S., unpublished.
(13) Antonio, M. R.; Xue, J. S.; Soderholm, L. *J. Alloys Compounds* **1994**, *207/208*, 444.
(14) Antonio, M. R.; Xue, J. S.; Soderholm, L., manuscript in preparation.

0897-4756/95/2807-0333$09.00/0

Table 1. Synthetic Conditions and Sample Characteristics for Ln_2MoO_6 (Ln = La, Ce, Pr, Nd, Sm, and Tb)

Ln	T_{max} (°C)/ duration (h)	cooling (°C/h)	color	symmetry
La	1250/40	furnace cooling	white	tetragonal
Ce	1200/72	250	black	cubic
Pr	1150/37	250	yellow	cubic
Nd	1200/40	250	green	cubic
Sm	1250/50	furnace cooling	yellow	monoclinic
Tb	1200/40	250	brown	monoclinic

The elucidation of this β-phase structure is the subject of an ongoing investigation.

We report here the results from neutron diffraction experiments on La_2MoO_6 and Tb_2MoO_6. The objective of this study is to address questions regarding cation and oxygen orderings in these materials. The superlattice lines observed in the X-ray, single-crystal study of La_2MoO_6 were very weak, a problem that was acknowledged in the previous structural work.[5] A confirmation of the suggested superstructure would have direct implications on La ion coordination and on possible mechanisms for polymorphic transformations between the three structural phases observed for this and related molybdate systems.[9] In addition, the confirmation of an acentric space group could have important technological implications. Neutron diffraction is an ideal technique to apply to this problem because of the relative simplicity of the structures under study and also because the added scattering power of oxygen relative to the heavy-metal ions should significantly increase the relative intensities of the superlattice lines. The structural characterizations of the α and γ phases of Ln_2MoO_6 compounds are expected to lead to a better understanding of the superstructure of the β phase.

Experimental Section

1. Synthesis. About 12 g Ln_2MoO_6 powder samples were prepared by mixing in an agate ball miller stoichiometric amounts of lanthanide oxides (i.e., La_2O_3, CeO_2, Pr_7O_{11}, Nd_2O_3, Sm_2O_3, and Tb_4O_7) with MoO_3. The mixtures were packed tightly into platinum containers (15 mm diameter and 120 mm long) by mechanical force. To exclude extra air in the container, the unusued portion of the container was flattened before sealing in air. The samples were heated in a tube furnace to the designated maximum temperature (T_{max}) within 6 h, soaked for at least 37 h, cooled at a rate of 250 °C/h to 200 °C, or followed by furnace cooling to room temperature. Details regarding the synthetic conditions and the characteristics of individual samples are given in Table 1. The final products were pulverized and the phase identifications carried out on a Scintag powder X-ray diffractometer using Cu Kα radiation.

2. Neutron Diffraction. La_2MoO_6 and Tb_2MoO_6 were selected for powder neutron diffraction experiments. They were packed into cylindrical vanadium cans with a diameter of 1.0 cm. Time-of-flight (TOF) neutron diffraction data were collected at room temperature using the general purpose powder diffractometer (GPPD) at Argonne's Intense Pulsed Neutron Source. For La_2MoO_6, data from back scattering detector banks of both $2\theta = 90°$ and 148° were refined simultaneously using the general structure analysis system (GSAS). Data from the 90° banks were used for Rietveld structure refinement of Tb_2MoO_6. The neutron scattering lengths used in the structure refinements were $b(La) = 0.827 \times 10^{-12}$ cm, $b(Tb) = 0.738 \times 10^{-12}$ cm, $b(Mo) = 0.695 \times 10^{-12}$ cm, and $b(O) = 0.5805 \times 10^{-12}$ cm.

(15) See, for example: Wells, A. F. *Structural Inorganic Chemistry*, 4th ed.; Oxford University Press: London, 1975; p 486.

Results

1. Synthesis of Polymorphs. Under standard solid-state synthetic conditions, La_2MoO_6 is most stable in tetragonal symmetry. No evidence was observed for the presence of either the α or the β phase, even as impurities. The Ln = Ce, Pr, and Nd materials prefer either the pseudocubic or the tetragonal structure, depending on the syntheses temperatures. For instance, a shining greenish crust and a yellowish core formed in a Pr_2MoO_6 pellet at 1200 °C. Powder X-ray diffraction revealed that the yellow core is a single-phase material structurally similar to that previously reported for the pseudocubic, or the β phase. The green crust is composed of primarily tetragonal γ phase, with a small amount of β phase. A single-phase sample of Pr_2MoO_6 with pseudocubic symmetry has been synthesized at 1150 °C. Therefore, the tetragonal form appears to be a high-temperature phase, whereas the cubic form is a lower temperature phase. Similar results have been obtained for Ln = Nd. For Ce_2MoO_6, a single-phase material that gives a pseudocubic X-ray powder pattern can be prepared at 1200 °C. A higher temperature synthesis, at 1250 °C, was attempted to see if the γ phase could be formed. The sample melted and the color changed from black to light brown. X-ray diffraction results indicate that the melt consists of a mixture of CeO_2 and other products. According to the above observations, the fluorite-like, pseudocubic structure is the only stable form for Ce_2MoO_6 under normal solid-state synthetic conditions. For the heavier or small lanthanides (Sm–Lu) and Y, a monoclinic α phase is the major product.

2. Crystal Structure Refinements of La_2MoO_6 and Tb_2MoO_6. The neutron diffraction powder patterns obtained from La_2MoO_6 are shown in Figure 1a,b. The first observation of note is that there are diffraction lines present in these patterns that are inconsistent with the previously reported[3] cell with $a = 4.089$ Å, $c = 15.99$ Å and space group $I\bar{4}2m$ (No. 121). These "extra" reflections occur at d spacings of 2.584, 2.403, 2.096, and 1.936 Å and have intensities approaching 20% of the most intense reflection. All reflections are consistent with the previously reported[5] cell of $a = 5.78$ and $c = 32.04$ and space group $I4_1/acd$ (or $I4c2$).

The principal task is to determine whether a centric space group $I4_1/acd$ (No. 142) or the acentric one $I\bar{4}c2$ (No. 120) favored by Efremov et al. best represent the data. This concern arises out of a previous report that La_2MoO_6 demonstrates a small piezoelectric effect,[5] indicating acentric symmetry. The two major differences between these two structures are that (1) there are two inequivalent La sites in the acentric structure such that they can move relative to each other (there are also two inequivalent Mo, but they remain constrained to the same relative positions in both space groups), and (2) the oxygens are less constrained in the lower symmetry space group. In other words, the extra peaks allowed in the acentric space group can have contributions from either La or oxygen ions. A close examination of the data reveals only lines that are indexable by the centric space group. That is, the extra lines permitted in the acentric space group have no

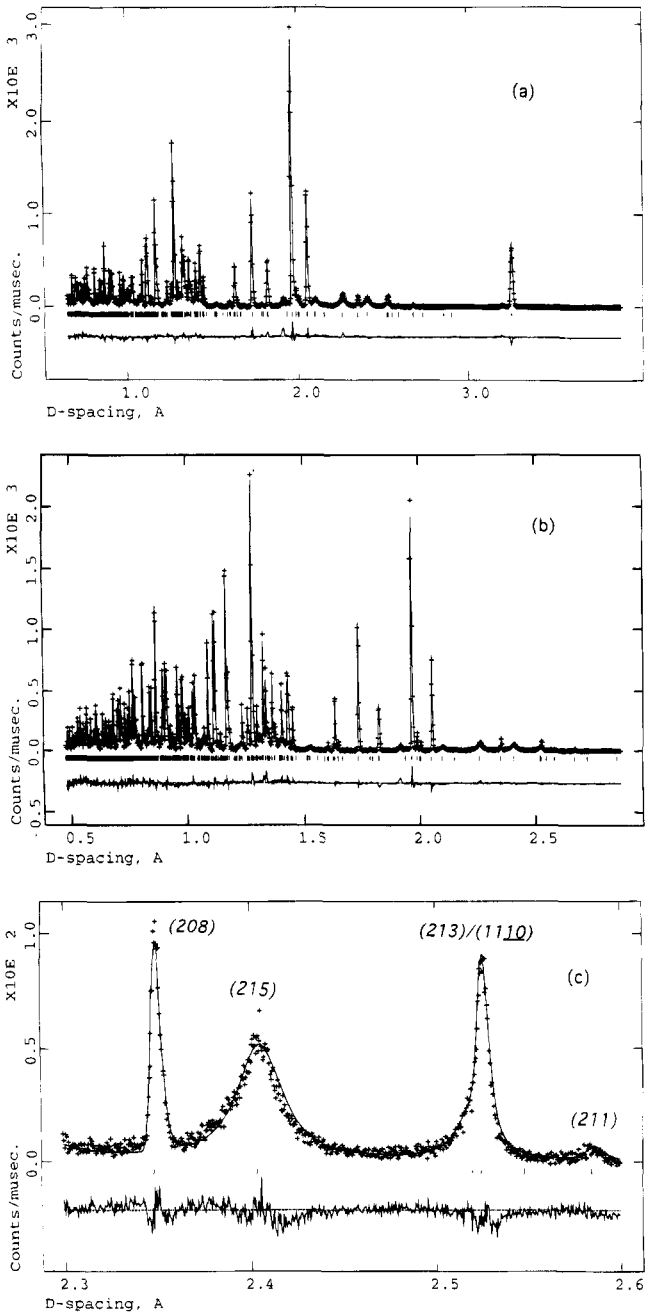

Figure 1. Rietveld refinement profiles at (a) 90° and (b) 148° data banks for La_2MoO_6. The plus (+) signs are the raw data of time-of-flight (TOF) neutron powder diffraction. Tick marks below the profile indicate the position of allowed Bragg reflections assuming the space group $I4_1/acd$ (No. 142). The solid line is the calculated profile. A difference curve (observed minus calculated) is plotted along the bottom. (c) Magnified view of broadened and normal reflection peaks in a selected d-spacing region of (b).

intensity associated with them. We also checked the acentric cell $I4_1/a$, previously reported for other, related lanthanide molybdates.[9] We found no extra lines consistent with this space group either. Therefore, because we have no information on which of the extra parameters required by the lower symmetry space group to refine, we chose to refine our data in the centric space group $I4_1/acd$, despite the previous report that La_2MoO_6 exhibits properties consistent with an acentric cell.

A close examination of the data presented in Figure 1a,b reveals a broadening of all the reflections in the (21l) zone relative to the other observed peaks, as shown

Table 2. Summary of Crystallographic Information for La_2MoO_6 and Tb_2MoO_6

	γ-La_2MoO_6	α-Tb_2MoO_6
crystal system	tetragonal	monoclinic
space group	$I4_1/acd$ (142)	$C2/c$ (15)
a (Å)	5.79701(3)	16.4554(3)
b (Å)		11.1143(2)
c (Å)	32.0353(3)	5.3936(1)
β (deg)	90	108.428(1)
Z	8	8
vol (Å^3)	1076.56	935.86(1)
density (g/cm^3)	5.79	7.24
formula wt	469.75	509.79
scale factor 1	10.37(6)	0.0071(2)
scale factor 2	11.99(6)	
extinction 1	78.3(24)	N/A
extinction 2	12.7(17)	
absorption	N/A	0.13(1)
observations	8116	2999
reflections	532	659
variables	43	96
R_{wp} (%)	7.25	2.97
R_{exp} (%)	3.26	2.32

in Figure 1c. It should be noted that these are exactly the same peaks that break the symmetry restrictions of the space group $I\bar{4}2m$. This broadening must be accounted for before any meaningful structural refinement can be undertaken. In this case, it is treated by using the third TOF profile function availabe in GSAS.[16] By assuming the broadened peak-shape function to be Lorentzian,[17] one can extract useful information by refining profile coefficients. Only the values of these coefficients can be used to identify whether the peak shape broadening is caused by an individual or a cumulative effect of the imperfections of powder samples, namely micro strain, particle size or stacking faults. The latter defect results in anisotropic particle size broadening. If the peak broadening was associated with microstrain in the sample, there would be a broadening in reciprocal space of each point that is proportional to the distance of the lattice point from the origin. In contrast, an isotropic particle size broadening makes all points the same size, independent of the distance from the origin. Therefore, by plotting a projection of h^*k^*0 planes in reciprocal space, we identify an anisotropic broadening axis of (001), and the stacking fault sublattice vectors of (001), (110) and (1$\bar{1}$0) that describe the subset of reflections that are *not* broadened. The other, namely the (21l) reflections should have a very large stacking fault coefficient γ_{sf} if the broadening *is* caused by a stacking fault. The refined stacking fault coefficients gave an average value of 110(2) μs/Å, whereas the coefficients for microstrain (γ1 and γ1e) and particle size (γ2 and γ2e) were refined to be close to zero. These results lead us to the conclusion that the peak shape broadening in this sample is caused by a stacking fault rather than microstrain or small, isotropic particle size effects. By definition,[18] the anisotropy in the domain size of this stacking fault can be calculated relative to the broadening axis with a parallel component of $P_{\parallel} = CK/(\gamma 2 + \gamma sf)$ and a perpendicular component of $P_{\perp} = CK/\gamma 2$, where C is the diffractometer constant (DIFC), and K is the Scherrerr constant, which is set to unity

(16) Von Dreele, R. B.; Jorgensen, J. D.; Windsor, C. G. *J. Appl. Crystallogr.* **1982**, *15*, 581.
(17) Von Dreele, R. B., 1990, unpublished.
(18) Larson, A. C.; Von Dreele, R. B. GSAS technical manual, **1990**, 121.

Table 3. Atomic Positions, Isotropic and Anisotropic Thermal Parameters ($\times 10^{-2}$ Å^2) for La_2MoO_6 Refined in Space Group $I4_1/acd$[a]

element	position	x	y	z	U_{iso}	U_{11}	U_{22}	U_{33}	U_{12}	U_{13}	U_{23}
La	*16d*	0.0	0.25	0.21142(2)	0.60(1)	1.09(11)	0.04(10)	0.66(3)	−0.09(6)	0.0	0.0
Mo	*8a*	0.5	0.25	0.125	0.98(2)	1.22(3)	1.22(3)	0.50(5)	0.0	0.0	0.0
O1	*32g*	0.3313(4)	0.0825(4)	0.08989(3)	1.22(2)	1.40(10)	1.24(9)	1.01(4)	0.02(3)	0.15(7)	−0.49(7)
O2	*16e*	0.2429(3)	0.5	0.25	0.67(2)	0.50(23)	0.80(23)	0.71(4)	0.0	0.0	−0.15(8)

[a] Anisotropic thermal parameters are defined as $T = \exp(h^2a^{*2}U_{11} + ... + 2hka^*b^*U_{12} + ...)$.

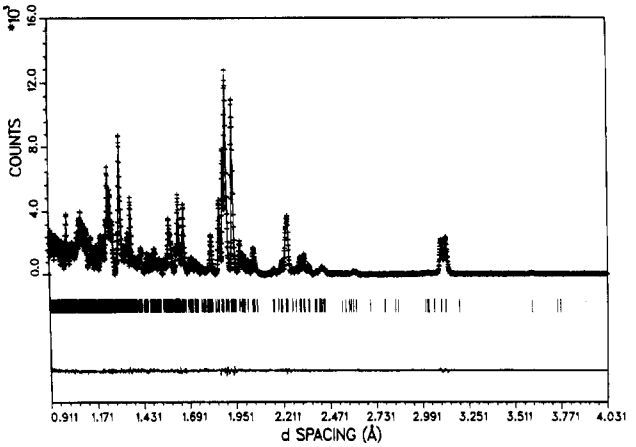

Figure 2. Rietveld refinement profiles for Tb_2MoO_6. The plus (+) signs are the raw TOF neutron powder diffraction data. The solid line is the calculated profile. Tick marks below the diffraction profile indicate the position of allowed Bragg reflections. A difference curve (observed minus calculated) is plotted at the bottom.

in this case. Since $\gamma 2$ is practically zero, the $P_\perp$ become infinite. This means that in real space, there are no observable stacking faults parallel to (001). The planes of stacking faults are perpendicular to (001). The calculated value of 82(2) Å for $P_{||}$ shows that the stacking fault has a boundary width of about every 2.5 unit cells along the *c* axis. Figure 1c shows a magnified view of the broadened (211), (213), and (215) reflections together with the sharp, normal (208) and (11$\bar{1}$0) reflections in the selected region of the 148° histogram.

The refinement of the neutron diffraction data obtained from La_2MoO_6, in space group $I4_1/acd$ and including the peak broadening parameters listed above, produce the parameters listed in Tables 2 and 3. The refined profiles of 90° and 148° histograms for La_2MoO_6 are shown in Figure 1a,b, respectively.

The structure of the monoclinic α phase of Tb_2MoO_6 was refined in space group *C*2/*c* (No. 15). A good agreement was reached between the results of TOF neutron diffraction refinement and those of X-ray diffraction reported previously.[7] The oxygen positions were determined more accurately in our experiments because of the relatively large contribution of oxygen to the neutron diffraction data. Anisotropic thermal parameters were refined, and no anomalous thermal ellipsoids were observed. The refined profile shown in Figure 2 demonstrates the excellent fit: $\chi^2 = 1.64$. The unit cells of Tb_2MoO_6, projected along (001) and (010), are illustrated in Figure 6a,b. Tables 2−7 give a summary of crystallographic information determined for La_2MoO_6 and Tb_2MoO_6, including the final positional and thermal parameters, as well as selected bond lengths and angles.

Table 4. Selected Bond Lengths (Å) and Angles (deg) of La_2MoO_6 in Space Groups $I4_1/acd$

		Bond Lengths			
La−La	×4	4.099(1)	Mo−Mo	×4	4.099(1)
	×4	3.809(1)		×4	5.797(1)
La−Mo	×4	4.008(1)			
La−O1	×2	2.715(2)	Mo−O1	×4	1.779(1)
	×2	2.708(2)		×4	2.944(1)
La−O2	×2	2.369(1)			
	×2	2.419(1)			
		Bond Angles			
O1−La−O1	×2	105.50(8)	O1−Mo−O1	×4	113.56(3)
O2−La−O2	×2	74.55(1)			
O1−La−O2	×2	95.03(4)			
	×2	95.51(2)			

Table 5. Atomic Positions and Isotropic Thermal Parameters ($\times 10^{-2}$ Å^2) for Tb_2MoO_6

atom	position	x	y	z	U_{iso}
Tb1	*4e*	0.5	0.1088(4)	0.75	0.44(10)
Tb2	*4e*	0.0	0.1336(3)	0.75	0.74(10)
Tb3	*8f*	0.3315(2)	0.1169(2)	0.1203(5)	0.40(7)
Mo	*8f*	0.1531(2)	0.1424(2)	0.4410(6)	0.58(7)
O1	*8f*	0.2335(2)	0.0520(3)	0.3663(7)	0.89(12)
O2	*8f*	0.0794(2)	0.0327(3)	0.4853(6)	0.68(9)
O3	*8f*	0.2274(2)	0.2034(3)	0.7392(6)	0.69(8)
O4	*8f*	0.1063(2)	0.2217(3)	0.1373(6)	0.83(9)
O5	*8f*	0.0728(2)	0.2642(3)	0.5853(7)	0.61(9)
O6	*8f*	0.5917(2)	0.0176(3)	0.5807(7)	0.86(10)

Table 6. Anisotropic Thermal Parameters ($\times 10^{-2}$ Å^2) of Tb_2MoO_6, Which Are Defined by $T = \exp(h^2a^{*2}U_{11} + ... + 2hka^*b^*U_{12} + ...)$

	U_{11}	U_{22}	U_{33}	U_{12}	U_{13}	U_{23}
Tb1	0.91(30)	0.86(30)	0.86(33)	0.0	0.82(24)	0.0
Tb2	0.34(27)	0.34(29)	0.76(28)	0.0	−0.20(24)	0.0
Tb3	0.73(20)	0.57(17)	0.21(22)	−0.30(18)	0.14(18)	−0.34(16)
Mo	0.62(20)	0.10(22)	0.35(17)	0.59(18)	−0.20(15)	0.41(19)
O1	0.16(22)	0.18(24)	0.23(30)	0.57(18)	0.46(17)	0.59(18)
O2	0.12(28)	0.18(36)	0.89(26)	−0.31(24)	0.40(23)	0.55(20)
O3	0.63(21)	0.11(23)	0.15(25)	0.12(21)	−0.36(18)	−0.21(20)
O4	1.28(30)	0.18(24)	0.10(26)	0.20(20)	0.53(21)	0.27(17)
O5	0.46(22)	0.24(25)	0.84(26)	−0.34(18)	−0.20(21)	−0.64(21)
O6	0.93(27)	0.84(31)	0.66(21)	−0.14(20)	0.19(19)	0.83(22)

Discussion

There are peaks in the neutron diffraction data obtained from La_2MoO_6 that rule out the space group $I\bar{4}2m$ originally reported[3] from an X-ray single-crystal study. Whereas our data includes no observable extra peaks to support the lower, acentric $I\bar{4}c2$ space group that was argued to be the correct space group[5] for La_2MoO_6, the data are consistent with the centric space group $I4_1/acd$. The relative atomic positions in the refined structure agree well with those previously reported,[5] although the space group is a supergroup of the previously chosen acentric one. The Tb_2MoO_6 neutron diffraction data and their refinement are consistent with the space group, *C*2/*c*, and refined parameters previously reported.[7]

The atomic size of the lanthanide ion appears to play a major role in determining the crystal symmetry in the

Table 7. Selected Bond Lengths (Å) and Angles (deg) in Tb_2MoO_6

		Bond Lengths (Å)			
Tb1–Mo	×2	3.684(5)	Tb1–O4	×2	2.770(5)
			Tb1–O5	×2	2.319(5)
			Tb1–O6	×2	2.223(5)
				×2	2.387(5)
Tb2–Mo	×2	3.449(4)	Tb2–O2	×2	2.377(6)
	×2	3.787(4)		×2	2.488(4)
	×2	3.898(5)	Tb2–O4	×2	2.478(5)
			Tb2–O5	×2	2.238(5)
Tb3–Mo	×1	3.528(4)	Tb3–O1	×1	2.499(5)
	×1	3.844(5)		×1	2.570(5)
	×1	3.913(6)	Tb3–O3	×1	2.426(6)
	×1	4.000(5)		×1	2.435(5)
	×1	4.104(5)	Tb3–O4	×1	2.655(5)
	×1	5.305(5)	Tb3–O5	×1	2.262(6)
			Tb3–O6	×1	2.213(6)
				×1	2.273(5)
Mo–O1	×1	1.796(5)	Mo–O1	×1	3.113(5)
Mo–O2	×1	1.799(6)	Mo–O2	×1	3.072(5)
Mo–O3	×1	1.812(6)	Mo–O3	×1	2.983(6)
Mo–O4	×1	1.805(6)			
Mo–O5	×1	2.214(6)			
Mo–Mo	×1	3.856(7)			
	×2	4.151(5)			
		Bond Angles (deg)			
O1–Mo–O2	×1	103.2(2)	O1–Mo–O3	×1	94.9(3)
O1–Mo–O4	×1	102.3(3)	O1–Mo–O5	×1	170.9(3)
O2–Mo–O3	×1	115.5(3)	O2–Mo–O4	×1	109.6(3)
O2–Mo–O5	×1	81.6(2)	O3–Mo–O4	×1	126.1(2)
O3–Mo–O5	×1	107.0(1)	O4–Mo–O5	×1	83.1(2)
O4–Tb1–O4	×1	94.2(2)	O4–Tb1–O5	×2	67.7(2)
O4–Tb1–O6	×2	105.6(1)	O5–Tb1–O5	×1	104.3(2)
	×2	121.9(2)	O5–Tb1–O6	×2	101.8(2)
O2–Tb2–O4	×2	107.9(1)	O2–Tb2–O5	×2	116.2(1)
	×2	93.0(1)		×2	124.2(1)
O4–Tb2–O5	×2	74.4(2)	O5–Tb2–O5	×1	99.0(3)
	×2	75.4(2)			
O1–Tb3–O3	×1	99.4(2)	O1–Tb3–O4	×1	119.0(2)
O1–Tb3–O5	×1	102.9(2)	O1–Tb3–O6	×1	90.7(2)
O3–Tb3–O4	×1	82.6(1)	O3–Tb3–O5	×1	120.8(2)
O3–Tb3–O6	×1	98.2(2)	O4–Tb3–O5	×1	71.5(2)
O4–Tb3–O6	×1	126.6(2)	O5–Tb3–O6	×1	104.8(2)

Ln_2MoO_6 system. The reason for this may be that small lanthanides such as Tb occupy less space. The crystal lattice accommodates this change by moving oxygens to low-symmetry sites. The extent of this crystal lattice distortion can be measured by the value of β angles of a monoclinic unit cell. A similar situation is observed in other structural series such as the perovskites.[15]

The determination of the centric space group $I4_1/acd$ for La_2MoO_6 has several implications important to understanding the physical and structural behaviour of these rare-earth molybdates. It has been previously noted that noncentric-type $\bar{4}2m$ phases constitute the parent structures from which the known ferroelectric molybdates are derived.[9] The originally reported $I\bar{4}2m$ space group places the La on a site with $2mm$ symmetry, where it is coordinated to six oxygens. In contrast, the space group $I4_1/acd$ has La 8-fold coordinated with oxygens. This coordination is very similar to that determined for Ce in Ce_2MoO_6 by the analysis of EXAFS data[13,14] and in fact similar to the coordination found for all the rare earths in this series.

The space group determined here is a supergroup of the sheelite $I4_1/a$ structure type observed previously for $Pr_2(MoO_4)_3$ and a supergroup of polymorphs of the other light lanthanides in the same series.[9] This is interesting because the phases Ln_2MoO_6 are sometimes found as impurities in their related $Ln_2(MoO_4)_3$ syntheses.[9] From the perspective of polymorphic phase transitions, the space group found for the Tb analogue Tb_2MoO_6, $C2/c$ is also a subgroup of $I4_1/acd$ (through $I4_1/a$), negating the necessity that there exists a first-order phase transition between the α and γ phases.

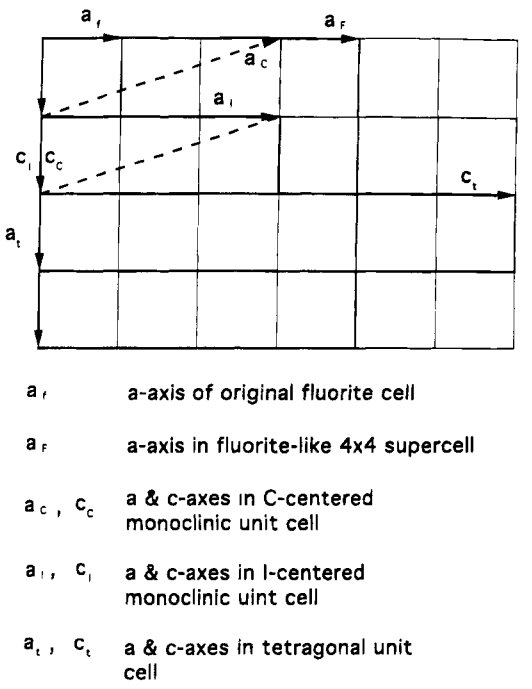

Figure 3. (010) projection of unit cells shows a simplified relationship of cell dimensions among various polymorphs of Ln_2MoO_6 and calcium fluorite structure.

The presence of polymorphic phases (α, β, γ) have now been determined for Pr-Sm in Ln_2MoO_6. Details of the structure are clearly dependent on the subtleties of syntheses. This result may serve as a possible explanation for the apparent discrepancies in the details of the published structures and physical properties of La_2MoO_6. The original two structures[3,5] were both done on single-crystal samples, whose preparative conditions were quite different than those used to make the powder samples studied here. It should be noted that the observed peaks that violate $I\bar{4}2m$ symmetry for La_2MoO_6 are the same reflections that are significantly broadened by stacking faults. Depending on the degree of broadening, this effect could be sufficient to render the weak X-ray peaks unobservable. It is interesting to speculate that the selective peak broadening observed in our sample may be the result of an incomplete phase transition that occurs during synthesis and may indicate that, under different synthetic conditions, crystals with $I\bar{4}2m$ symmetry may be obtained. If this were the case, then our inability to find evidence to support an acentric space group would not be inconsistent with the previous report that La_2MoO_6 exhibits a weak piezoelectric electric effect and no second harmonic generation[5] in some samples.

In principal, all the polymorphs in the Ln_2MoO_6 system can be regarded as derivatives of a calcium fluorite structure with different cation layer packing and anion rearrangements. A simplified diagram of the relationship of unit-cell dimensions of the fluorite structure and various Ln_2MoO_6 polymorphs is illustrated in Figure 3. The square at the upper-left corner represents the original cubic fluorite cell with an a-axis length of $a_f \approx 5.4$ Å. All the cations in this structure are eight-coordinated, and the anions are four-coordi-

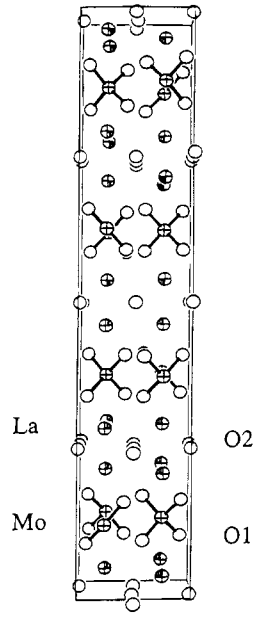

Figure 4. Unit cell for La_2MoO_6 in space groups $I4_1/acd$ (No. 142). The open ellipsoids represent oxygens.

nated. The tetragonal unit cell (or the γ phase) is composed of six fluorite units with $a_t \approx a_f$ and $c_t \approx 6a_f$. A C-centered monoclinic unit cell is described by the dashed lines with cell axes labeled as a_c and c_c. The body-centered monoclinic unit cell marked with a_I and c_I is also shown in Figure 3. It deviates slightly from an orthorhombic symmetry (about 1° from 90°). The dimensions of the two monoclinic unit cells are related by $a_I \approx (a_c^2 - c_c^2)^{1/2}$, $b_I \approx b_c$ ($\approx 2c_I$), and $c_I \approx c_c$. Also illustrated in Figure 3 is one possible cubic supercell of the β phase, which extends to four fluorite cells in all three dimensions and has an a-axis length of $a_F \approx 4a_f$.

Besides the apparent similarities existing among the three Ln_2MoO_6 polymorphs and fluorite structure, the details of each polymorph may be very different. The crystal structure of La_2MoO_6 can be regarded as two La_2O_2 layers sandwiched between layers of MoO_4 tetrahedra as shown in Figure 4. The La ions in La_2MoO_6 are coordinated by eight oxygens. These La–O bonds are not all equal as is typical in the fluorite structure. Instead there are four short La–O2 and four long La–O1 bonds. The four short La–O2 bonds are 2.369 Å (×2) and 2.419 Å (×2) long, and the four longer La–O1 bonds are 2.708 Å (×2) and 2.715 Å (×2) long, as shown in Figure 5a. These eight oxygens form a staggered configuration along the (001) projection. The Mo ions can be considered as four-coordinate (when only those oxygens in the first coordination sphere are taken into account) with Mo–O1 bond lengths of 1.779 Å as shown in Figure 5b. Although the MoO_4 units have one bond length for all four Mo–O1 bonds, they are distorted tetrahedra. The Mo sit on sites of $\bar{4}$ (S_4) symmetry, so that the angles of O1–Mo–O1 (113.56° and 101.56°) deviate from the tetrahedral (T_d) angle of 109.4°. As shown in Figure 4, the O2 layers are located between two La layers, which give rise to two sets of short La–O2 bonds. The O1 atoms are bonded with both La and Mo atoms. A strong Coulombic attraction from highly electropositive Mo^{6+} ions may pull the O1 atom away from the La ions and may be the source of the lengthening of La–O1 bonds and the twisting of LaO_8 cubes.

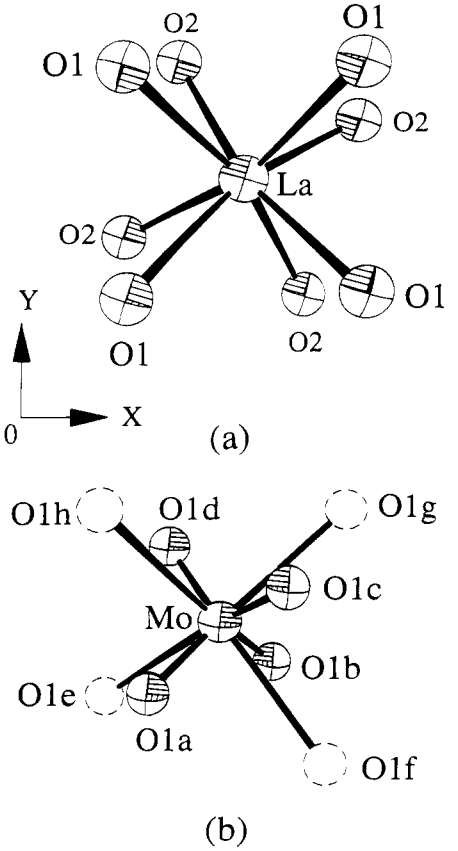

Figure 5. Clusters of LaO_8, MoO_4, and "MoO_8" in La_2MoO_6. (a) LaO_8 cluster viewing along (001). (b) "MoO_8" cluster.

The space group determined for Tb_2MoO_6 is a subgroup of that reported for La_2MoO_6. It can be best described as four zigzag, one-dimensional MoO_5 polyhedral rows per unit cell running through the TbO_8 polyhedral framework along (001), as shown in Figures 6a,b. The Tb ions in the TbO_8 polyhedra are in a more distorted coordination environment than those La ions in La_2MoO_6: Tb1 ions have three sets of short Tb1–O bonds and only one set of long bonds (Tb1–O4 of 2.770 Å); for Tb2, all the Tb2–O bond lengths are in the short range; in the case of Tb3, all the Tb3–O bonds are different lengths and angles. The lattice distortion results in the lengthening of a few bonds (i.e., Tb1–O4) and the shortening of the rest of the Tb–O bonds. As expected, the averaged Tb–O bond length of 2.412 Å is shorter than that of La–O (2.553 Å). The molybdenum tetrahedra are also seriously distorted. The oxygen that resides in the second coordination sphere of Mo in La_2MoO_6 is now so close to the Mo ions in Tb_2MoO_6 (2.214 Å) that MoO_5 clusters are created. The two dimensional MoO_4 and double Ln_2O_2 layers along the a,b plane found in La_2MoO_6 no longer exist in the monoclinic structure. All the MoO_5 pseudo-square pyramids in the α phase share corners with TbO_8 polyhedra and form two consecutive mixed-metal oxide layers $(Tb/Mo)O_2$ along the bc plane. Several structural features are of interest here. First, the average Mo–O bond length of 1.803 Å (1.885 Å if the fifth oxygen were taken into account) in the Tb_2MoO_6 compound is longer than that of 1.779 Å in the La_2MoO_6 compound, despite the fact that the former has a smaller unit cell volume than the latter. This phenomenon can be understood by the fact that a mixed occupation of lanthanide and molybdenum ions occurs in the same layer: the MoO_5

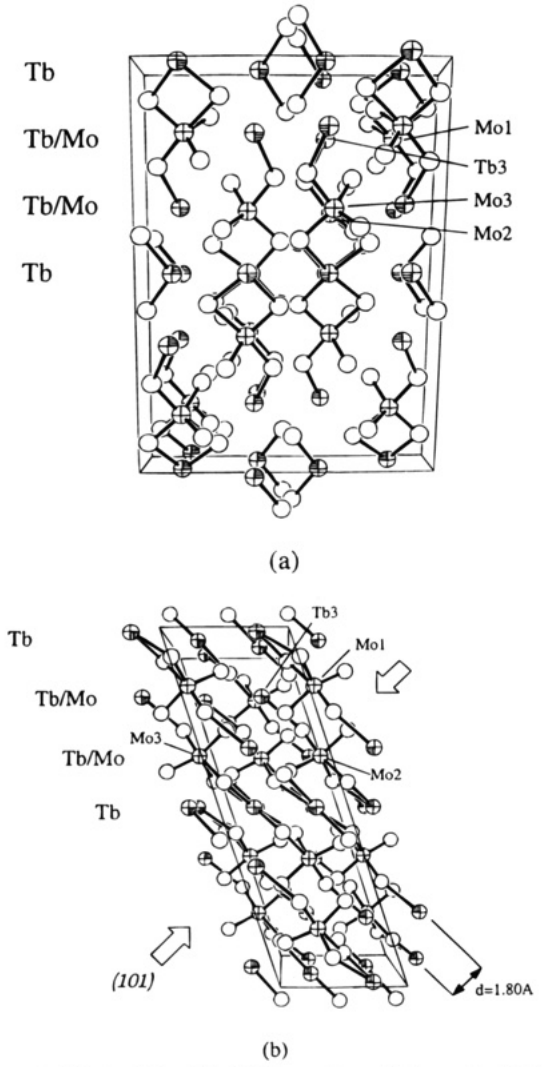

Figure 6. Unit cells of Tb_2MoO_6 projected along (a) (001) and (b) (010). The open ellipsoids represent oxygens.

square pyramids occupy less volume than do the LnO_8 polyhedra. In addition, both the MoO_4 tetrahedra in La_2MoO_6 and the MoO_5 polyhedra in Tb_2MoO_6 are in a *discrete* state. In other words, they are connected to LnO_8 polyhedra but do not share oxygens among themselves. This may supply structural grounds for the insulating behavior observed in most of the Ln_2MoO_6 compounds. Finally, if those oxygens in the second coordination sphere are counted as "bonded" to the Mo ions, there are no longer MoO_4 or MoO_5 units, but the "MoO_8", units that occur in the fluorite structure. Figure 5b demonstrates that the Mo ions in La_2MoO_6 could become eight-coordinate if those oxygens (indicated by dashed ellipsoids in the figure) bonded to the separated Mo neighbors in the same MoO_4 layer are taken into account. These oxygens are normal to the faces of the MoO_4 tetrahedron with a long distance of 2.944 Å from the Mo ion. A similar but more distorted situation is seen in Tb_2MoO_6, where the oxygens O1b, O2b, and O3b can be considered as "bonded" to the Mo ions (see Figure 7b). The long Mo−O bond lengths are in the range 2.983−3.113 Å. It will be interesting to see if there is any relationship between the proposed MoO_8 polyhedra and the semiconducting behavior of Ce_2MoO_6 (β phase).

To understand the mechanism of polymorphic phase transitions in the Ln_2MoO_6 compounds, a comparison

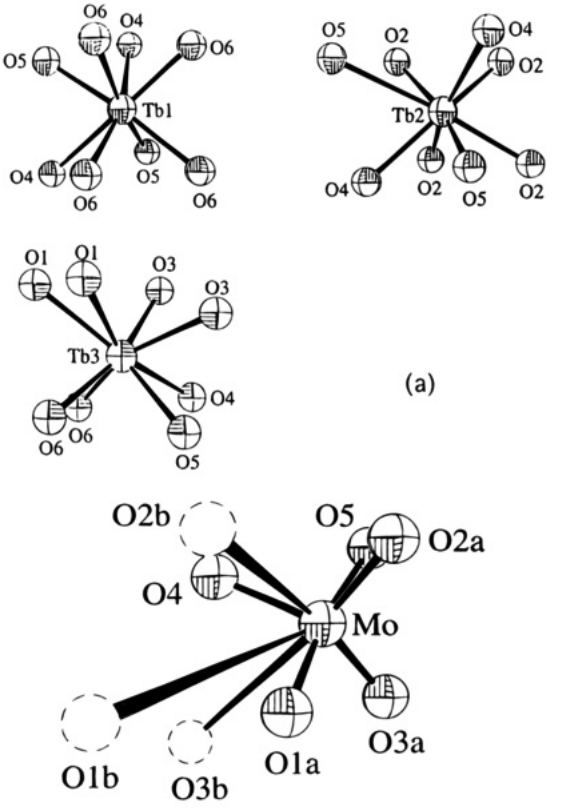

Figure 7. Clusters of TbO_8, MoO_5, and "MoO_8" in Tb_2MoO_6. (a) The three TbO_8 as distorted cubes. (b) "MoO_8" clusters.

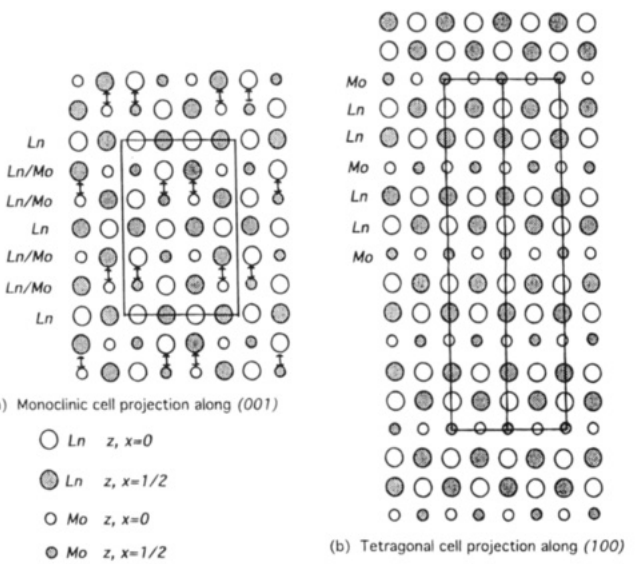

Figure 8. Comparison of crystal structures of La_2MoO_6 and Tb_2MoO_6.

of cation layer stacking sequences between the α and γ phases is made in Figure 8. The layer stacking sequence along the a axis of the α phase can be written as ...-LnO_2−[$(Ln/Mo)O_2$]$_2$−LnO_2−... and for γ phase, ...−MoO_4−Ln_2O_2−MoO_4−.... The latter can be derived from the former via an exchange of certain Ln and Mo ions in the two adjacent Ln/Mo mixed layers. The exchange directions are shown by arrows in Figure 8. A better understanding of the possible route of this exchange may be obtained by a closer examination of the crystal structure of Tb_2MoO_6. For example, Tb3 may exchange with several neighbor Mo ions, such as

Mo1, Mo2, and Mo3. Since the monoclinic lattice is squeezed along the (101) direction, the distance between the adjacent (101) layers is shortened (around 1.80 Å as shown in Figure 6b). This structural distortion gives rise to a closest Tb3–Mo1 distance of 3.53 Å. An exchange between these two ions will not lead to a layer stacking sequence of the γ phase but, instead, to a disorder of cations that should not be favored from a thermodynamic sense. The most likely exchange probably occurs between Tb3 and Mo2 because (i) the distance between these two ions is 3.84 Å, which is shorter than that of Tb3–Mo3 (3.91 Å), (ii) they are corner-sharing polyhedra, and (iii) they are in the same (101) layer. With knowledge of the cation orderings in the α and the γ phases, we can assume that the Mo and Ln ions in the β phase may be more well-ordered than that of the α phase but more disordered than that of the γ phase. This assumption is supported by the analysis of Ce[13] and Mo[14] EXAFS for Ce_2MoO_6. Assuming that the β phase represents a transitional one between the α and γ phases, the LnO_8 framework should be similar to those two phases whereas the ordering of MoO_n will be different. It will be interesting to find out if the n value in MoO_n is close to 4 or 5. The polymorphic transitions of $\alpha \leftrightarrow \beta \leftrightarrow \gamma$ observed for the Ln_2MoO_6 compounds are more likely accomplished via a cluster-exchange mechanism involving MoO_4, LnO_8, or more complex species.

Conclusions

Several compounds of the Ln_2MoO_6 family with Ln = La, Ce, Pr, Nd, Sm, and Tb have been prepared. The crystal structures of La_2MoO_6 and Tb_2MoO_6 have been studied by using TOF neutron diffraction. A centric space group $I4_1/acd$ (No. 142) has been assigned to La_2MoO_6. The $(21l)$ peak shape broadening in the diffraction profile has been analyzed according to a stacking fault model. The crystal symmetry of the Ln_2MoO_6 compounds are determined by the interplay among the atomic size of Ln and synthesis temperature. The α phase seems most stable for small lanthanides at low synthetic temperatures whereas the γ phase is preferred by large lanthanides. The polymorphic phase transitions of $\alpha \leftrightarrow \beta \leftrightarrow \gamma$ occurring in the Ln_2MoO_6 system is discussed in terms of a metal–oxygen cluster-exchange mechanism.

Acknowledgment. The authors gratefully acknowledge J. W. Richardson and R. L. Hitterman at Argonne National Laboratory for valuable assistance and R.B. Von Dreele at Los Alamos National Lab for inspiring discussions on the stacking fault model. This work is supported by the U.S. DOE, BES-Chemical Sciences, and has benefited from the use of the Intense Pulsed Neutron Source at Argonne National Laboratory, all under Contract W-31-109-Eng-38.

CM940390M